HEFAT2012
9th International Conference on Heat Transfer, Fluid Mechanics and Thermodynamics
16 – 18 July 2012
Malta

INVESTIGATION OF THE PRESSURE DISTRIBUTION OVER A MAV MODEL

Kamoushi H.* and Soltani M.R.
*Author for correspondence
Department of Aerospace
Science and Research Branch
Islamic Azad University
Tehran, Iran
E-mail: hadikamoushi@yahoo.com

ABSTRACT

An intensive experimental study was conducted to investigate the effects of various parameters on the surface pressure distribution of a Zimmerman type wing wildly used for MAVs. A full scale wing was designed, fabricated, and tested in a low speed, low turbulence wind tunnel. The model cross section was an airfoil of a type which is usually used in MAV wings. The wing planform was of Zimmerman type.

The model was equipped with several static pressure ports located at different span-wise and chord-wise sections of the wing. Surface static pressure data at various angles of attack ranging from -10 to 20 degrees, and at three different Reynolds numbers equal to that of the full scale model were obtained. It should be noted that to author's knowledge, no experimental pressure data for this type of wing having an airfoil in its cross section are available in the literature.

All data that the authors were able to find, dealt with aerodynamic force and moment of a flat plate wing of Zimmerman planform. The measured pressure data over the wing surface shows several interesting results which are different from those for the conventional wing planforms, i.e., rectangular, triangular, etc.

NOMENCLATURE

V_∞	[m/sec]	Freestream velocity
V	[m/sec]	Local velocity
AR	-	Aspect ratio (b^2/S)
b	[m]	Wingspan
S	[m^2]	Wing area
Re	-	Reynolds number ($\frac{V_\infty C}{\nu}$)
c	[m]	Wing chord
ν	[m^2/sec]	Kinematic viscosity
C_p	-	Pressure coefficient
$C_{L_{max}}$	-	Maximum lift coefficient
C_{L_α}	-	Lift-Curve slope
$\propto_{stall}$	Degree	Stall angle of attack
L/D	-	Lift-to-Drag ratio
α	Degree	Angle of attack

Abbreviation	
LAR	Low aspect ratio
A.O.A	Angle of attack
L.E.	Leading edge
T.E.	Trailing edge
BR	Blockage ratio
max	Maximum
min	Minimum

INTRODUCTION

About ten years ago Micro Air Vehicles (MAVs) have been seriously proposed in academic and industrial centers of many countries. As a result several MAVs of various kinds (fixed wing, flapping and rotary wing) have been designed, built and operated and even have been used by some countries in military and civil fields. MAVs that have been designed so far all have the following criterions;

- A range of about 1.5 kilometers.
- Max length and width of 15 centimeters
- Min endurance of 30 minutes
- Max stall speed of 10 m/sec
- Able to carry a payload of at least 18 grams
- Full-automatic or at least semiautomatic
- Able to use by amateurs

Considering these specialties, MAVs operate at Re number from 5×10^4 to 2.5×10^5 and have very low AR wing, AR≅1. Thus the role of the aerodynamic is obvious because if there is an optimal aerodynamic design for MAV, it can be hopeful to attain most of the above requirements.

Low aspect ratio (LAR) wings extensively researched at higher Re numbers in the form of delta wings at subsonic, transonic and supersonic speeds. Many of these studies are focused on the high A.O.A aerodynamics of delta and other

types of pointed LAR wings. For MAVs, delta wing planforms are not ideal because for a given max dimension, delta wings offer less lifting area (and therefore less payload capability) than a rectangular or circular wing of the same max dimension [1].

Between 1930 and 1950 Zimmerman, Bartlett and Vidal, and Wadlin et al. performed experiments on LAR wings, although at significantly greater Re numbers. Theoretical and analytical theories of LAR wing aerodynamics have been performed by Bollay, Weinig, Bera and Suresh, Polhamus, and Rajan and Shashidhar and perhaps the most complete analysis and review of LAR wings was performed by Hoerner in his two-volume series on lift and drag [1].

The latest studies on LAR wings at low Re number are related to Torres and Mueller experiments on a number of flat plate models of varying planform shapes; rectangular, elliptical, Zimmerman (formed by joining two half-ellipses at either the quarter-chord location) and inverse Zimmerman (formed by joining two half-ellipses at either the three-quarter-chord location) type all of which flat plate with AR of 0.5, 1 and 2 (Figure 1). Their tests were conducted at Re numbers of 7×10^4 and 10^5 [1]. Considering this research, it can be said that for $AR \leq 1$ and the mentioned Re number, rectangular and inverse Zimmerman planform have the best results for lift and they have greater $C_{L_{max}}$ but the drag of the rectangular wing was more than that of the other planforms, especially at low Re numbers; In addition from their L/D versus A.O.A data for all the planforms with $AR \leq 1$, the inverse Zimmerman wing efficiency was more than that of the other planforms.

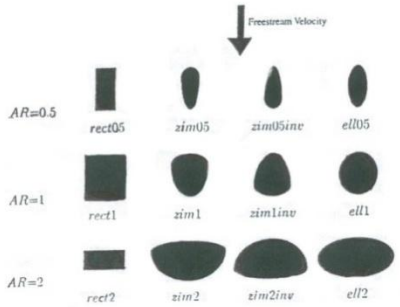

Figure 1 Various wing planform shapes

Flow visualization results from Torres and Muller study for rectangular and inverse Zimmerman planforms with $AR \leq 1$, revealed that wingtip vortices separate from the wing and from each other at the maximum wingspan location and they effect much less the flow on the wing. Other result of this research is increase of C_{L_α} and $\propto_{stall}$ as AR is reduced and lack of rational decrease of $C_{L_{max}}$ along the wingspan for the inverse Zimmerman wing. However the most aerodynamic efficiency has been related to the inverse Zimmerman shape with $AR \leq 1$. This planform has been used as the lower wing (main wing) of a fixed wing MAV (Figure 1) with a special airfoil in the present experimental work.

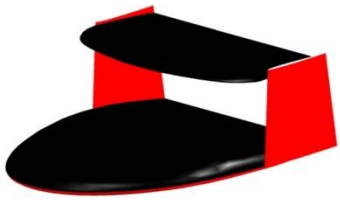
Figure 2 Isometric view of MAV configuration

EXPERIMENTAL APPARATUS

All experiments are conducted in a subsonic wind tunnel of open circuit type with a test section size 457 ×457 ×1200 mm operating at speeds ranging from 5 to 33m/sec. The settling chamber of the tunnel has a 7.3:1 contraction ratio with anti-turbulence screens and honeycomb to reduce the tunnel turbulence to less than 0.1 percent in the test section (Figure 1).


Figure 3 Wind tunnel used for the present work

From the maximum dimensions of the MAV lower wing (Figure 1), dimensions of the test section, max A.O.A in this experiments (20 degree) and very low Blockage Ratio (BR), about 5%, a model with a scale of 1:1 has been designed and manufactured where its lower wing section has an airfoil similar to that of GOE 723 one (Figure 1 and 6). Its upper surface is covered with a total of 36 pressure orifices of 0.6mm diameter arranged in five different span wise rows, section 1 ($\frac{2y}{b} = 0$), section 2 ($\frac{2y}{b} = 0.3$), section 3 ($\frac{2y}{b} = 0.5$), section 4 ($\frac{2y}{b} = 0.7$), and section 5 ($\frac{2y}{b} = 0.9$) (Figure 1 and 8).

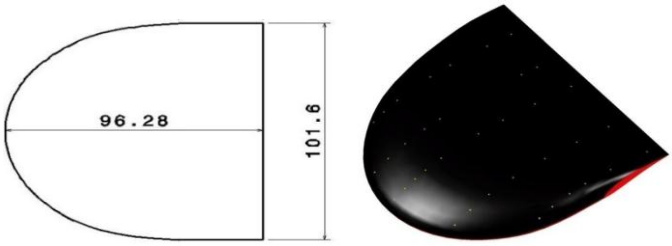

Figure 4 Schematic of the MAV lower wing and its top view (dimensions in mm)

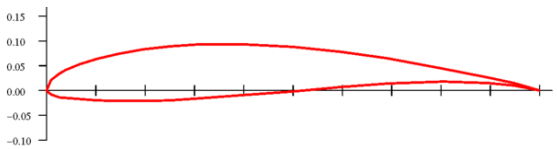

Figure 5 MAV lower wing airfoil section

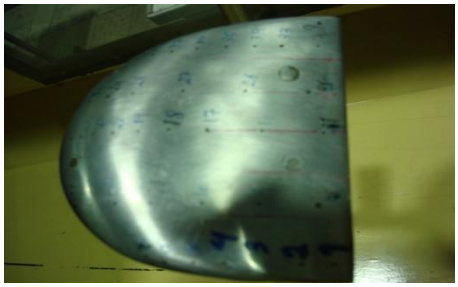

Figure 6 MAV lower wing in the test section

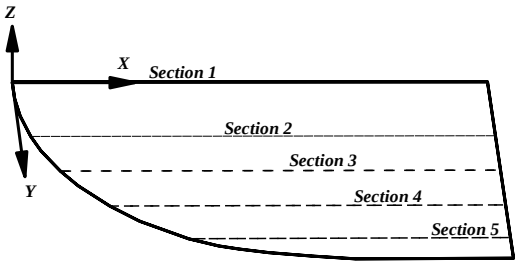

Figure 7 Location of pressure orifices on the lower wing

36 differential pressure transducers have been used for measuring the static pressure over the lower wing surface. These sensors are very accurate and their differential pressure limits are ± 5 mbar. Each transducer data is collected via a terminal board and transformed to the computer through a 64 channel, 12-bit Analog-to-Digital (A/D) board capable of an acquisition rate of up to 500 kHz. The experiments were conducted at 3 speeds 10, 15 and 20 m/s (respectively equal to 3 Re numbers 7×10^4, 10^5 and 1.4×10^5 based on the max chord length). The angles of attack were varied from -10 to 10 degrees with step of 2 degree and from 10 to 20 degrees with step of 1 degree. Using the method of ref. 3, both the single sample precision and the bias uncertainty in each measured variable were estimated and subsequently propagated into the C_p variations. The max overall uncertainty calculated in this way for the C_p data was less than ±4% of the total C_p values.

DISCUSSION OF RESULTS

Results from the wing upper surface pressure distribution at various speeds and A.O.A and at the mentioned Re numbers, are shown in table 1 and in the related figures. It should be noted that the region over the wing surface where $\frac{dC_p}{dx} < 0$, called favourable pressure gradient where creates suction over the wing surface. The region over the wing surface where $\frac{dC_p}{dx} > 0$, called adverse pressure gradient where the $|C_p|$ decreases but the value of C_p increases positively.

As shown in Figure 1, the wing surface is divided into the 4 regions for better description of the pressure distribution and its variations.

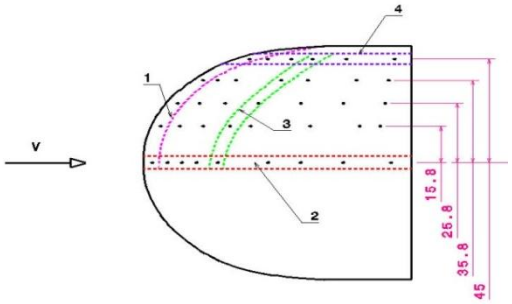

Figure 8 Pressure orifices and four regions on the upper surface of the MAV lower wing

Region 1 has been drawn parallel to the L.E. toward the wing tip and it contains the closest pressure orifices to the L.E. In this region the cross-flow behaviour along the leading edge from the center toward the wing tip will be survied.

Region 2 is located exactly at the center line, at the section of the wing which has the maximum thickness to chord ratio, and has been extended from the L.E. to the T.E. and is used to survey the flow behaviour at the center line of the wing.

Region 3 is located at the wing center and has been extended to the wing tip parallel to the L.E. to survey the cross-flow behaviour from the center toward the wing tip.

Region 4 is located near the wing tip and has been extended to the T.E. to survey the flow behaviour and the effects of the tip vortices.

Region 1

As shown in table 1 and Figures 9, 10 and 11, for $0 \leq 2y/b \leq 0.3$ the pressure coefficient pressure gradient decrease as the A.O.A increases. For $0.3 < 2y/b \leq 0.5$ the pressure coefficient is still negative, but the pressure gradient gradually become positive as the A.O.A is increased. For $0.5 < 2y/b \leq 0.7$ the pressure coefficient has become negative while the pressure gradient has remained almost constant as the A.O.A is varied. Finally for $0.7 < 2y/b \leq 0.9$ the pressure coefficient is negative but the pressure gradient become positive as the A.O.A increases. It may be said that transfer of the position of the stagnation point toward the wing lower surface, the L.E. sweep, rate of decrease of the wing thickness and also the flow quality can affect the cross-flow quality in the Region 1.

By comparing the C_p distribution for a fixed A.O.A with each other while the freestream velocity is varied, it is clearly seen that the pressure coefficient for all the points of region 1 increases positively as the freestream velocity has bean increased. This is probably due to the reduction of the ratio of the local velocity on the model to the free stream velocity, (V/V_∞).

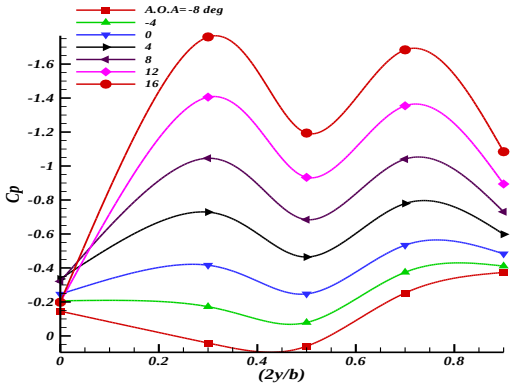

Figure 9 Effect of A.O.A on the pressure distribution of region 1, $V_\infty = 10\, m/sec$

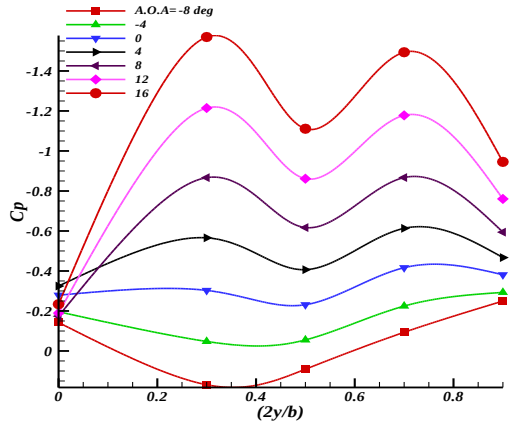

Figure 10 Effect of A.O.A on the pressure distribution of region 1, $V_\infty = 15\, m/sec$

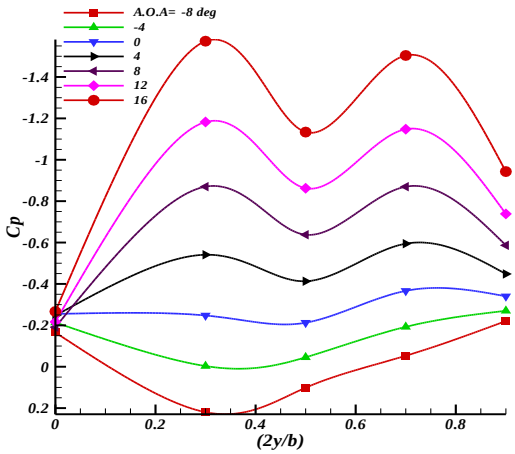

Figure 11 Effect of A.O.A on the pressure distribution of region 1, $V_\infty = 20\, m/sec$

Region 2

As shown in table 1 and Figures 12, 13 and 14, it is clearly seen that for positive angles of attack pressure coefficient decreases in front portion and increases for $X/C > 0.2$. No sign of flow separation over this region at all angles of attack is seen from these figures. Increasing the freestream velocity increases the magnitude of C_p for almost all angles of attack, however, no significant change in the C_p distribution is observed. C_p distribution for this part of the wing differs significantly with those of region 1 discussed previously. Because of transfer of the position of the stagnation point toward the wing lower surface, maximum pressure point gradually is removed as the A.O.A increases.

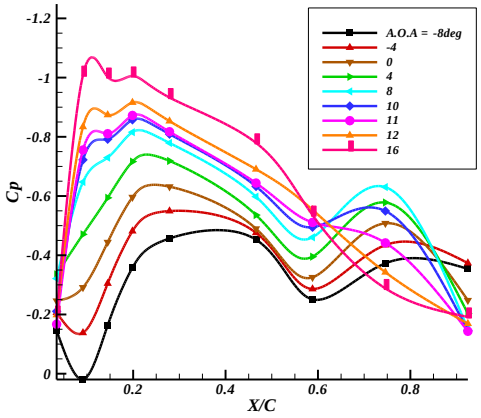

Figure 12 Effect of A.O.A on the pressure distribution of region 2, $V_\infty = 10\, m/sec$

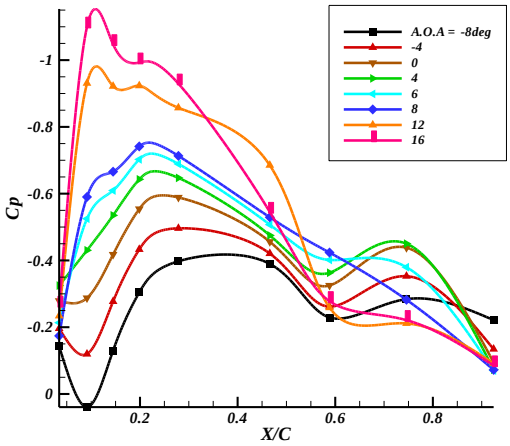

Figure 13 Effect of A.O.A on the pressure distribution of region 2, $V_\infty = 15\, m/sec$

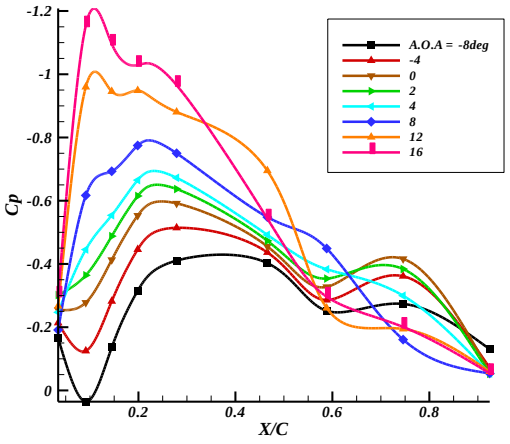

Figure 14 Effect of A.O.A on the pressure distribution of region 2, $V_\infty = 20\, m/sec$

Region 3

Since this region has been located parallel to region 1, its pressure distribution expects to be similar to that of region 1. However, since this region is further from the L.E and less flow impressibility from the L.E. sweep and vortices, the variations are smoother. It might be concluded that the cross-flow quality in region 3 is affected by the L.E. sweep and by the rate of decrease of the wing thickness. As shown in table 1 and Figures 15, 16 and 17, the distribution for $0 \leq 2y/b \leq 0.4$, for all cases are almost similar to those of region1, however, for the rest, $0.4 \leq 2y/b \leq 0.9$, the variation differs. For $V_\infty > 10\,m/s$ and for angles of attack $\propto > 4$ degrees, the flow over a portion of the wing surface, $2y/b \geq 0.5$, has a very low pressure which is probably caused by formation of tip vortices. These vortices create largt C_L and remain attach over the wing surface, hence their existence is desirable. However, for the low angles of attack case, $\propto < 8$ degrees, these vortices are not present and the flow seams to be in the verge of separation in the mentioned region, $2y/b \geq 0.5$.

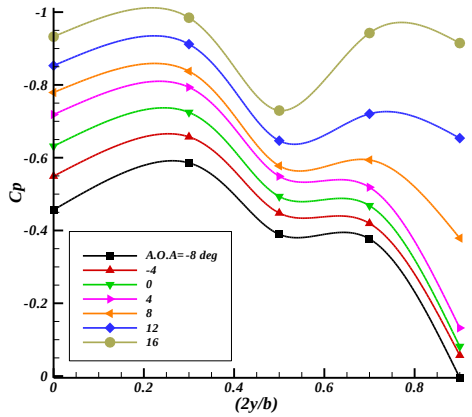

Figure 15 Effect of A.O.A on the pressure distribution of region 3, $V_\infty = 10\,m/sec$

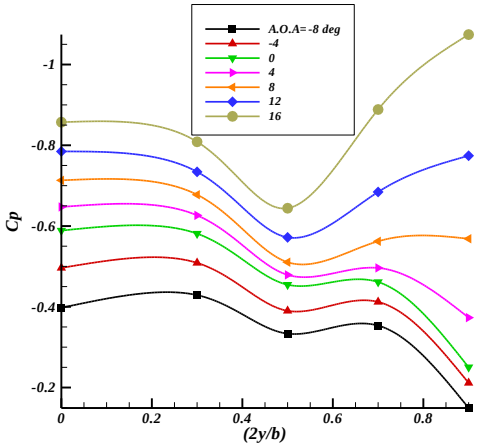

Figure 16 Effect of A.O.A on the pressure distribution of region 3, $V_\infty = 15\,m/sec$

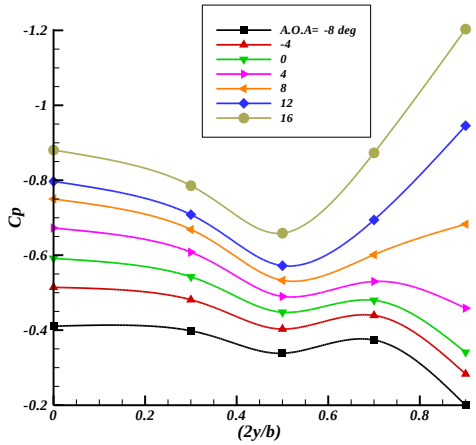

Figure 17 Effect of A.O.A on the pressure distribution of region 3, $V_\infty = 20\,m/sec$

Region 4

As shown in table 1 and Figures 18, 19 and 20, for all velocities and angles of attack tested, C_p is almost constant over a portion of this region and except for the $V_\infty = 20\,m/s$ case, C_p increases sharply followed by a decrease, these change behavior of C_p distribution is due to the formation and probably burst, at high angles of attack, of the tip vortices that formed in this region. For $V_\infty > 10\,m/s$ a portion of this region is covered with vortical flow too, or the effect of tip vortices has caused C_p to decrease in this region for these angles of attacks. For $\propto < 8$ degrees, $|C_p|$ continues to decrease as X/C increases from $X/C \geq 0.4$.

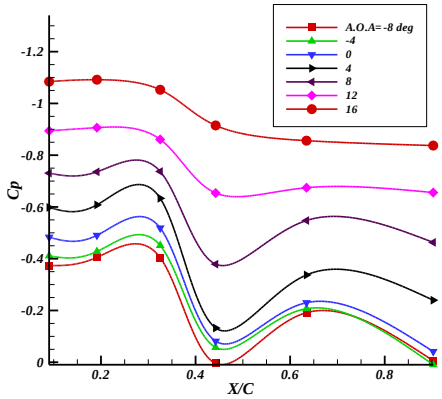

Figure 18 Effect of A.O.A on the pressure distribution of region 4, $V_\infty = 10\,m/sec$

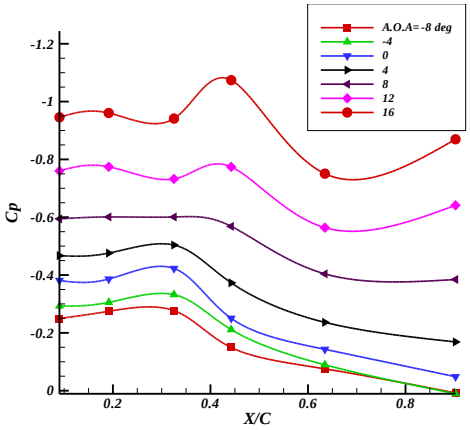

Figure 19 Effect of A.O.A on the pressure distribution of region 4, $V_\infty = 15\ m/sec$

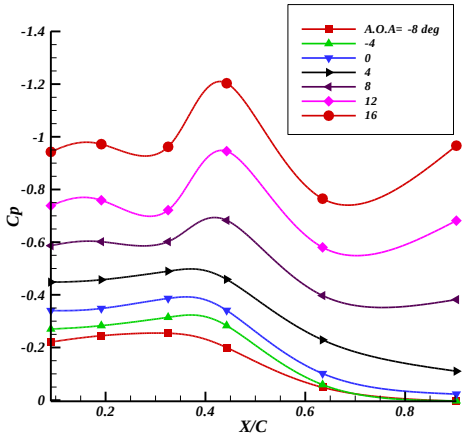

Figure 20 Effect of A.O.A on the pressure distribution of region 4, $V_\infty = 20\ m/sec$

CONCLUSION

An experimental study on the surface pressure of a Zimmerman type wing at various angles of attack and freestream velocity was conducted. The results show that the pressure distribution on the upper surface of the wing, is influenced by the L.E. sweep angle, wing airfoil and its L.E. radius and rate of change of the wing thickness are the most important factors which affect the flow quality on the wing. Surface pressure distribution over this type of wing is completely different from those of the standard planform wings; l.e, trapezoidal, rectangular, etc. The flowfield over the wing surface is seams to be strongly affected by the tip vortices forming at moderate to high angles of attack. No distinct flow separation was observed over the wing surface even at 16 degrees angle of attack. Freestream velocity has significantly effect on the C_p distribution of portions of the wing surface. More tests are needed to better understand and quantify the complex flow field over the wing of such planforms.

References

[1] Mueller, T. J., "Fixed and Flapping Wing Aerodynamics for Micro Air Vehicle Applications", T. J. Mueller, Ed., 1th Ed., Vol. 195, 8 Jan 2002, pp. 115-134.

[2] Pope, A., Rae, W., and Barlow, J., "Low Speed Wind Tunnel Testing", 3rd Ed., Wiley, New York, 1999.

[3] Thomas, G.B., Roy, D.M. and John, H.L.V., "Mechanical Measurements", Fifth Edition, Addison-Wesley Publishing Company (1993).

Table 1 Effect of velocity and A.O.A on the low wing upper surface pressure distribution

	10m/s	15m/s	20m/s
-8deg	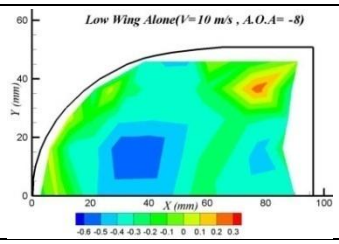	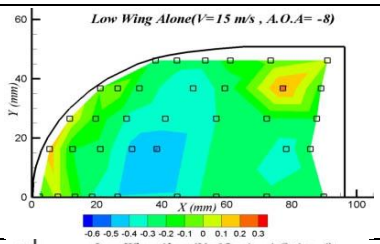	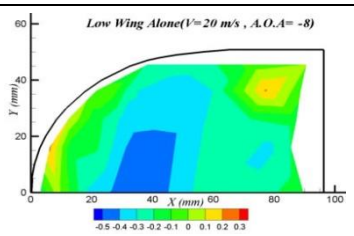
-4deg	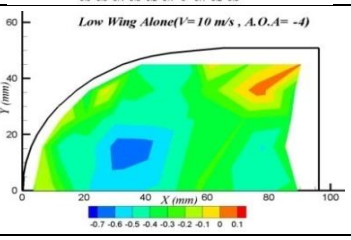	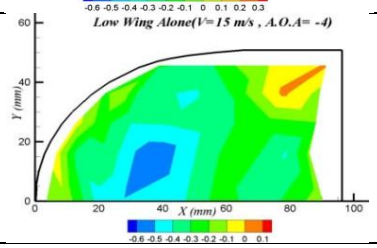	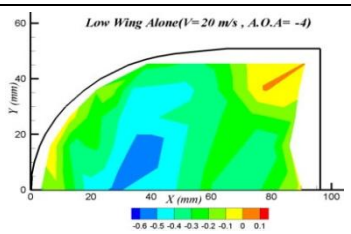
0deg	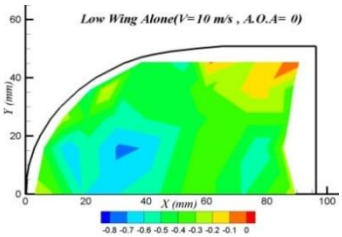	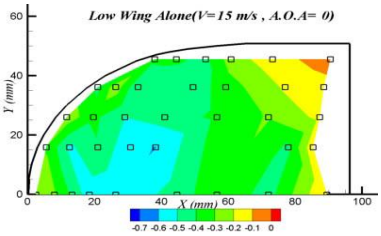	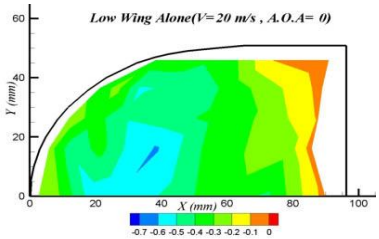
4deg	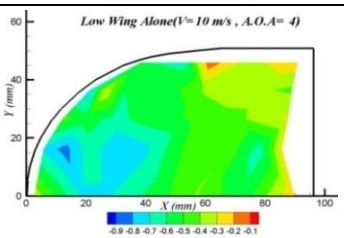	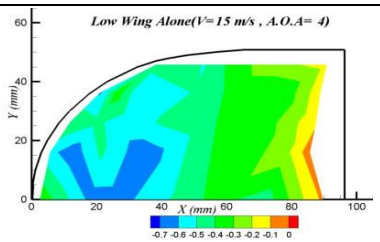	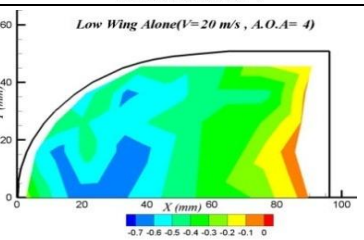
8deg	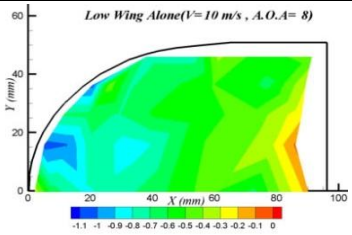	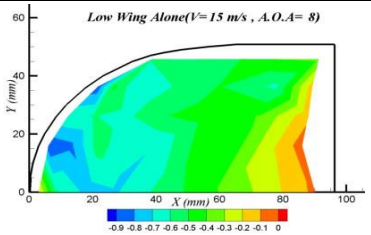	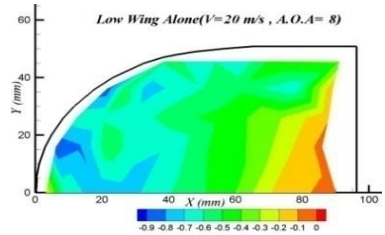
12deg	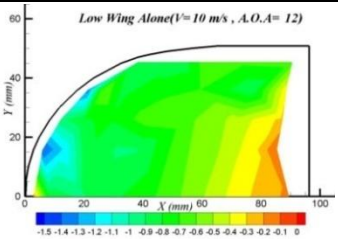	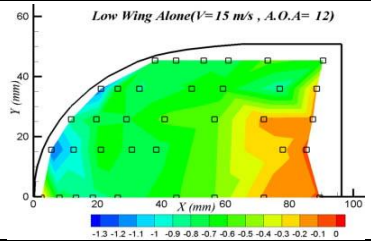	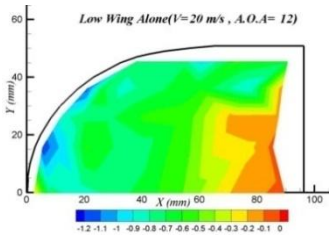
16deg